Numerical and experimental analysis of the vacuum corn seed degassing system

George Ipate , Filip Ilie * , Viorel Fătu , Gheorghe Voicu

Posted Date: 11 January 2024

doi: 10.20944/preprints202401.0908.v1

Keywords: degassing process; corn seeds; vacuum chamber; modeling; simulation; structural dynamic analysis

Article

Numerical and Experimental Analysis of the Vacuum Corn Seed Degassing System

George Ipate [1], Filip Ilie [2,*], Viorel Fatu [1] and Gheorghe Voicu [1]

[1] Department of Biotechnical Systems, National University of Science and Technology Polytechnic Bucharest, Spl. Independentei 313, 060042 Bucharest, Romania; puiu.ipate@gmail.com; fatu_viorel@yahoo.com, ghvoicu_2005@yahoo.com

[2] Department of Machine Elements and Tribology, Polytechnic University of Bucharest, Spl. Independentei 313, 060042 Bucharest, Romania; ilie.filip@yahoo.com;

* Correspondence: ilie.filip@yahoo.com

Abstract: In this work, the degassing process of corn seeds was experimentally and numerically analyzed by removing air or other gases from around the seeds, specifically from the seed coating, in a rough vacuum chamber. The two complementary variants are employed to understand and optimize this process to improve the quality and germination rate of the seeds. Several experiments were conducted with well-established durations and masses of corn seeds at different temperatures to observe and record the behavior of the system, facilitating the modeling of the degasification process in the vacuum compartment. Modeling the degasification operation in the vacuum chamber allowed for determining the pressure profiles on the vacuum chamber and its lid. Numerical simulations were either conducted using a simulation program developed in the Visual Basic Applications (VBA) language for Microsoft Excel to model the degassing process in the vacuum chamber, or with the assistance of specialized software (transient structural analysis and simulation program in the ANSYS Workbench environment). Statistical analysis of the correlation between experimental and estimated pressure values revealed that both the proposed mathematical model and the solution method are well-chosen, with differences expressed through the absolute error (EA) being very small. Structural dynamic analysis carried through the Finite Element Method (FEM) highlights that the chosen materials for manufacturing the vacuum chamber vessel (316 stainless steel) or the chamber lid (transparent acrylic plastic) are durable and capable of withstanding the desired pressure and temperature demands in the seed treatment process. Additionally, through structural dynamic analysis, it was possible to study the deformation of system components, providing a detailed perspective on their structural distribution.

Keywords: degassing process; corn seeds; vacuum chamber; modeling; simulation; structural dynamic analysis

1. Introduction

Treating seeds in vacuum chambers is a procedure used to boost the quality and germination rate of seeds. This method involves exposing the seeds to an environment with reduced pressure for the complete elimination of air around them in a special chamber called a vacuum chamber [1], [2], [3], because:

- By removing the air (degassing) around the seeds, oxidation and decomposition are prevented, contributing to their long-term preservation;
- Seeds become more permeable, allowing them to absorb treatment evenly and more efficiently, facilitating the subsequent absorption of water and nutrients necessary for germination [4];
- The vacuum environment can help destroy, eliminate harmful microorganisms, or reduce the number of pathogens and pests that may be present on the surface of the seeds, potentially affecting germination and plant health [3], [5];

 doi:10.20944/preprints202401.0908.v1

- Vacuum treatment can activate certain enzymes in seeds, accelerating the biochemical processes necessary for germination [6];
- By using vacuum treatment, the required quantity of treatment substances can be minimized, reducing waste and potential environmental impact [7], [8].

The retention of essential elements in the seed is appropriately regulated and sheltered by physical and chemical barriers facing external biotic factors. This nutrient package is indispensable for germination, leading to the development and replication of plants [4].

The vacuum treatment process can vary depending on the plant species and treatment objectives. Generally, seeds are placed in a special vacuum chamber where atmospheric pressure is reduced or eliminated [9], and this can be achieved through a vacuum system or by evacuating the air from a sealed chamber. Physical treatments are challenging to implement as there is a delicate balance between effectively eradicating seed-transmitted diseases and causing harm to the seeds [7], [10]. Not all seed batches react the same way to all treatments, making it difficult to predict how physical treatments will affect seed germination and vigor [5], [9], [11], [12], [13]. Chemical treatments that do not have phytotoxic effects on seeds are available, but methods for complete internal penetration have not been identified [7], [10].

Treating seeds in vacuum chambers is commonly used in agricultural and horticultural settings to improve seed quality and germination rates, leading to enhanced crop yields and plant health [1], [12]. However, it is crucial to ensure that seed treatment is carried out with appropriate equipment and under controlled conditions to avoid seed damage or the onset of undesirable negative effects. Seed treatment practices must always adhere to safety and environmental regulations.

In a complete vacuum, the temperature of the air cannot be measured in the usual sense, as a vacuum represents a space devoid of matter, including air particles [14]. Temperature is a measure of the average kinetic energy of molecules in a system. The absence of particles in a vacuum makes it impossible to measure the usual temperature of air, as there are no particles to generate thermal motion or interact with a thermometer. There are only concepts related to radiation and radiant temperature, which are different from the air temperature encountered under normal conditions [12].

On the other hand, in a vacuum system, there are primarily three sources of gas, known as the gas load, namely [15]: residual gas in the system, vapors in equilibrium with the present materials, gases produced or introduced by leaks (also, "virtual leaks" of captured gas without penetration through the walls), degassing (adsorption), permeability (gas transfer through a solid, through porous materials, glass, etc.). Therefore, in this work, vacuum pressure testing was performed through dynamic Finite Element Method (FEM) analysis of the system designed for treating corn seeds. Thus, the degassing process of corn seeds was experimentally and numerically analyzed by removing air or other gases from around the seeds, specifically from the seed coating, in a vacuum chamber. The goal was to understand and optimize the process, as well as to improve the quality and germination rate of the seeds. This was achieved by modeling the degassing process in the vacuum chamber using specialized software (transient structural analysis and numerical simulation program in the ANSYS Workbench environment developed in the Visual Basic Applications language). The correlation between experimental and estimated pressure values revealed, through statistical analysis, that both the proposed mathematical model and the solution method are well-chosen, with differences expressed by the absolute error (EA) being very small.

2. Materials and Methods

Experimental analysis and numerical simulations of the degassing process of seeds in a vacuum chamber are complementary methods used to understand and optimize this process. Degassing involves removing air or other gases from around seeds or products, which is crucial in various fields such as the food industry, pharmaceuticals, or space technology.

For this, the seeds are first cleaned and sorted to remove any debris, damaged seeds, or foreign materials. They are then placed inside the vacuum chamber in a way that ensures uniform distribution and avoids overcrowding. The chamber is sealed, and a vacuum with low pressure is created, aiding in the removal of air bubbles and ensuring consistent treatment for all seeds. While

Preprints (www.preprints.org) | NOT PEER-REVIEWED | Posted: 11 January 2024 doi:10.20944/preprints202401.0908.v1

the seeds are in the vacuum, various substances or treatments that promote growth or beneficial microorganisms can be applied. After the treatment is complete, the chamber is filled again with ordinary atmospheric air by releasing the vacuum.

The experimental analysis was conducted in a setup whose schematic is presented in Figure 1a, and Figure 1b illustrates the porous structure of corn seeds, allowing the observation and recording of seed behavior under vacuum conditions.

The seeds are deposited in the container of the vacuum compartment, and then the pressure inside it is gradually reduced until reaching the desired vacuum pressure using the vacuum system (see Figure 1). Subsequently, various parameters are monitored, such as the degassing rate, the quantity of gases eliminated, and changes in the volume of the seeds, etc.

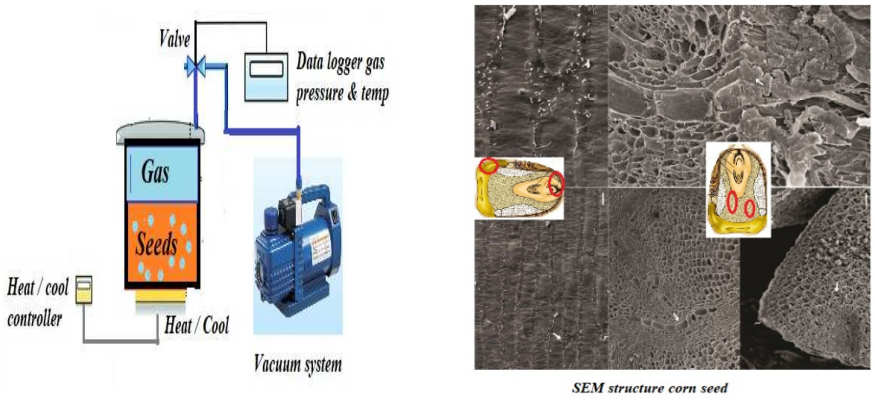

(**a**) (**b**)

Figure 1. Experimental setup and SEM structure of corn seeds: (a) schematic of the vacuum treatment setup; (b) porous structure of corn seeds.

The experimental results can deliver useful knowledge about the efficiency of the degassing process, the time required to achieve a certain degree of degassing, and other relevant aspects. On the other hand, numerical simulations can be conducted using specialized software, with programs for structural analysis and Computational Fluid Dynamics (CFD) for fluid dynamics analysis.

For the experimental analysis, 5 experiments were performed, each lasting 10 minutes, using a mass of 5 kg of corn seeds at different temperatures (27.7, 20.3, 14.2, 8.5, and 4.8°C) to observe and record the system's behavior.

To perform a numerical simulation, data about the vacuum chamber geometry, material characteristics of the seeds and gases, as well as initial and boundary conditions, are required.

Simulations can aid in visualizing gas flows around the seeds and provide detailed information about the time needed to achieve a certain degree of degassing, pressure distribution, temperature, etc. Using simulations, virtual tests can be conducted to optimize the vacuum chamber's geometry or evaluate different degassing strategies, thus reducing costs and time required for real experiments.

Both experimental analysis and numerical simulations contribute to a deeper and more comprehensive understanding of the seed degassing process in a vacuum chamber. The obtained results can be used to enhance the process and make informed decisions in designing and optimizing degassing systems.

Analysis of mechanical elements or assemblies through the Finite Element Method (FEM) primarily unfolds in three distinct stages, according to Figure 2 [16], [17], [18]:

1. Pre-processing - where the model is defined (by constructing a mathematical model applied to a 3D geometric element created with CAD software and divided into smaller bodies) that is to be analyzed, along with the ambient environmental factors applied to it;
2. Analysis and solving (mainly carried out on computers with high computing power);
3. Post-processing of results (using powerful graphic visualization devices) involves analyzing and interpreting the results, as well as identifying issues in the studied structure.

Preprints (www.preprints.org) | NOT PEER-REVIEWED | Posted: 11 January 2024 doi:10.20944/preprints202401.0908.v1

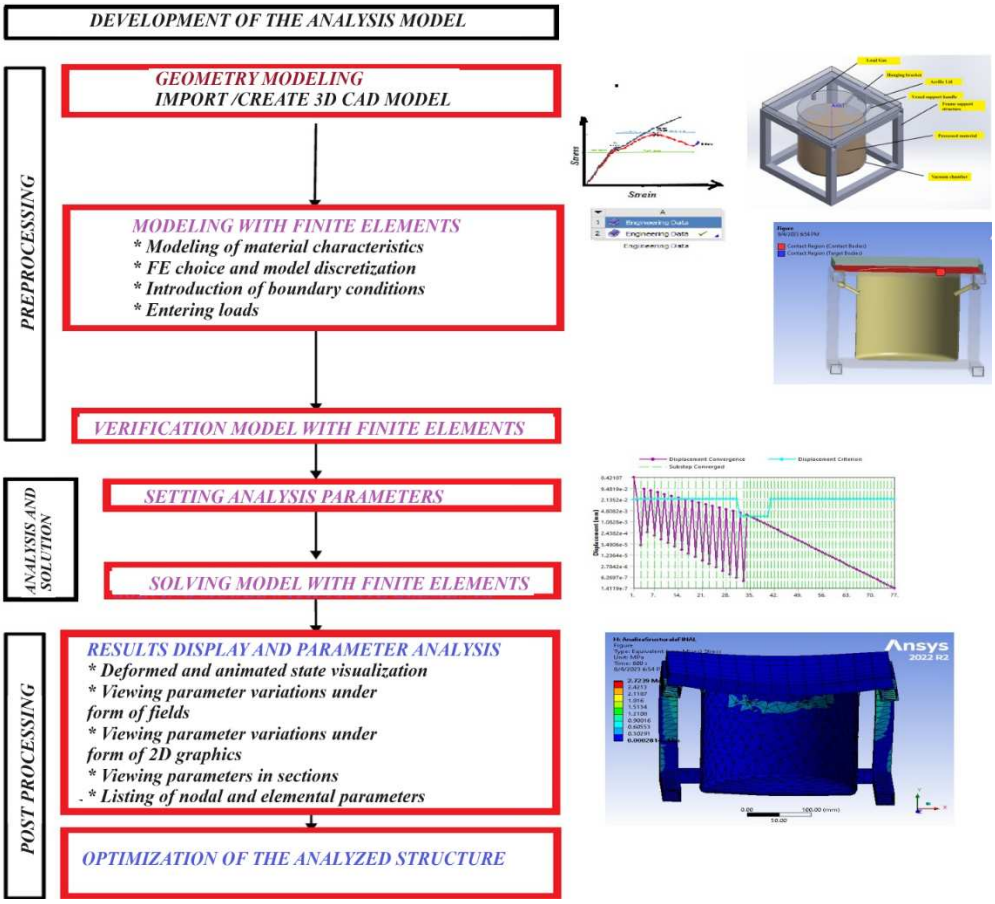

Figure 2. Stages of finite element analysis.

The approximate nature of the FEM outcomes from the fact that the real geometry is always replaced with a mesh of finite elements that approximates the real shape but cannot reproduce it accurately due to the finite number of elements. The unknowns of the problem are calculated only at the nodes of the structure. The formulation of the FEM is based on formulating the extreme conditions that some quantities involved in the studied phenomenon must satisfy. Therefore, it is a numerical method with a wide range of applicability that benefits from the advantage of a simple formulation [19].

The 3D geometric modeling of the vacuum seed treatment system was designed in SolidWorks 2022, while the structural analysis is performed using the ANSYS - Workbench software. ANSYS - Workbench is a software platform that combines basic solving capabilities with a set of product management tools for effective handling of elements and data.

The design and construction of the vacuum chamber took into consideration three main components: (1) their arrangement; (2) the vacuum structure; and (3) the heat exchange system. In this work, the first two components will be described and analyzed. The vacuum space was constructed and manufactured to meet the following requirements:

- provide the necessary conditions to achieve specific processing conditions for cereal seeds (such as removing dust particles before applying a thin layer of fungicides, insecticides, and bactericides, and evaporating water from the material for conditioning);
- be capable of maintaining elevated and cold temperatures for an extended period;
- Produce a vacuum environment that encompasses pressures from atmospheric down to 100 Pa at a minimum;
- have an interior size of at least 20 liters.

To achieve a higher level of vacuum (i.e., lower pressures), special systems and pumps are used to evacuate more gas from the system. The lower the pressure, the fewer gaseous particles the space contains, which is crucial in many scientific and technological applications.

Preprints (www.preprints.org) | NOT PEER-REVIEWED | Posted: 11 January 2024 doi:10.20944/preprints202401.0908.v1

Thus, the vacuum chamber was fabricated from one-piece cast 316 stainless steel, highly durable, and capable of withstanding temperatures as low as -70°C, with the chamber's lid made of acrylic Plexiglas. This material was chosen for being ordinarily applied in the manufacturing of thermal vacuum containers due to its high resistance [9]. The material for the chamber vessel has the following characteristics: density of 7.985e-006 kg/mm^3, Poisson's coefficient of 0.25, Young's modulus of 1.95e+005 MPa, stiffness of 1.3e+005 MPa, shear strength of 76,923 MPa. The lid material has the following properties: density of 1.185e-006 kg/mm^3, Poisson's coefficient of 0.3952, elastic modulus of 3,225 MPa, stiffness of 5,182.9 MPa, shear strength of 1,167.9 MPa.

The vacuum chamber has a cylindrical vessel structure with dimensions specified in Table 1 (outer diameter of 240 mm, height of 240 mm, and wall thickness of 3 mm). Based on structural analysis using FEM, the 3 mm thickness of the vessel wall ensured the required constructive integrity for the vessel. The end plate of the chamber not only exhibits high strength and impact resistance but also provides sufficient visibility to observe the interior state. The thick and transparent lid, made of acrylic material with a thickness of 15 mm, is equipped with a silicone ring for effective sealing [13].

Figure 3 illustrates the physical system created for this study, and the technical specifications of the vacuum chamber and lid are presented in Table 1.

(**a**) (**b**)

Figure 3. Vacuum system: (a) side view, (b) top view.

Table 1. Technical specifications of the vacuum chamber.

Maximum rated vacuum	482.6 mmHg at sea level	**Maximum operating temperature**	70 °C
Volume	20 L	**Lid dimensions (diameter x thickness)**	240x15 mm
Length of steel wire hose	1250 mm	**Dimensions of the vacuum chamber (diameter x height x thickness)**	240x240x3 mm

To obtain the required vacuum pressure inside the vessel, a low-pressure pump was employed. The vacuum pump is a rotary vane mechanical pump (Value, 2020) with a maximum rotation speed of 1440 rpm, a power of 200 W, and a flow rate of 42 l/min at 220V/50Hz. The pump has the necessary capabilities for high vacuum, is equipped with a built-in manometer to measure rough vacuum, and can reach pressures in the range from atmospheric pressure to 20 Pa. To quantify medium and high vacuum pressures inside the vessel, a portable Testo 552 device was implemented, as shown in Figure 4.

Preprints (www.preprints.org) | NOT PEER-REVIEWED | Posted: 11 January 2024 doi:10.20944/preprints202401.0908.v1

Figure 4. Portable device for measuring vacuum pressure.

It is a requirement for production equipment to be tested before its initial operation to predict the behavior of processed materials, often valuable components. This is achieved by simulating real physical process conditions. Process equipment components must also withstand extreme pressure and temperature conditions for years. As maintenance work during this period consumes significant material resources, all components produced must be fully reliable.

3. Results and Discussion

3.1. Analytical and numerical modeling

a) Finite element mathematical modeling

The developed mathematical model applies to dynamic systems with a finite number of degrees of freedom through the analytical formulation of structure dynamics with added damping. The analytical model of this formulation (the matrix differential equation of vibrational motion) is the one from classical dynamic analysis. In this context, loads or loading conditions vary over time and are applied instantaneously. Dynamic loads involve oscillating weights, impacts, collisions, and unpredictable amounts, and therefore, this case it supposes involve [20]:

- transient dynamic evaluation, employed to calculate the feedback of a structure to external loads that fluctuate unpredictably over the period.

In dynamic analysis, the matrix equations for force equilibrium are applied to a dynamic system [20], [21]:

- for a structure without foreign load:

$$[M] \times [\ddot{X}(t)] + [C] \times [\dot{X}(t)] + [K] \times [X(t)] = 0 \quad (1)$$

- for a system with an external load:

$$[M] \cdot [\ddot{X}(t)] + [C] \cdot [\dot{X}(t)] + [K] \cdot [X(t)] = [F(t)] \quad (2)$$

where: M - mass; $\ddot{X}$ - acceleration; C - Rayleigh damping; $\dot{X}$- velocity; K - stiffness; X – displacement and F – load (all variabels are in matrical form), t - time.

By solving the equations (1) and (2), we can obtain the natural frequencies of a structure. The types of loads used in a static analysis are the same as those of a dynamic. The expected results from the software include natural frequencies, displacements, deformations, and stresses. All these outcomes can also be acquired in the total deformation, where δ_t is a scalar quantity, and:

$$\delta_t = \sqrt{\delta_x^2 + \delta_y^2 + \delta_z^2}, \quad (3)$$

where $\delta_{x,y,z}$ - the components of deformation along coordinate axes can be obtained in either global or local coordinates.

The associated differential equation has the form [15]:

$$\mathbf{M}^{+} \cdot \ddot{X}(t) + \mathbf{C}^{+} \cdot \dot{X}(t) + \mathbf{K}^{+} \cdot X(t) = \mathbf{F}^{+}(t), \quad (4)$$

Preprints (www.preprints.org) | NOT PEER-REVIEWED | Posted: 11 January 2024 doi:10.20944/preprints202401.0908.v1

in which the matrices and vectors are specific to the dynamic model with added mass (M^+) connected to the primary system through elastic connections (stiffness coefficient K^+), damping connections (damping coefficient C^+) and F^+ - appropriate load.

b) Numerical modeling

Here is presented an approach to mathematical modeling established on the utilization of computational instruments for numerical simulations [22]. The process involves transitioning from problem formulation and equation establishment to the implementation of computational algorithms and analysis of results.

Due to the factors depicted beyond an evaluation of the pumping time should fundamentally differ for evacuating a vessel in the rough vacuum region compared to evacuating in the regions of medium and high vacuum.

In the case of gas evacuation of a vessel in gross vacuum mode (excluding supplementary quantities of gas or vapor), the effective pumping speed, s_{ef} of the pump-vacuum chamber assembly, depends only on the required pressure, p (after time t), on the volume, V of the chamber and the pumping time, t.

Accompanied by an invariable pumping speed, s_{ef} and supposing that the maximum pressure reached, p_f (the final/desired pressure) by the chosen pump model, is such that $p_f \ll p$, the pressure drop over time, p(t) in a vessel of vacuum is provided by the differential equation of the first order [2]:

$$-\frac{dp}{dt} = \frac{s_{ef}}{V} \cdot p \qquad \text{or} \qquad \frac{dp}{p} = -\frac{s_{ef}}{V} dt, \tag{5}$$

which by integration, considering that the pressure varies from the initial pressure, p_0 = 1,003 mbar at the time $t = 0$ to a minimum value, p (after the time, t), then the effective pumping speed, s_{ef} could be estimated as a function of the pumping time, t from equation/relation (5) as follows:

$$\int_{1003}^{p} \frac{dp}{p} = -\frac{s_{ef}}{V} \cdot t \Rightarrow ln\frac{1003}{p} = -\frac{s_{ef}}{V} \cdot t, \tag{6}$$

where from result:

$$s_{ef} = \frac{V}{t} \cdot ln\frac{1003}{p}. \tag{7}$$

Noting $ln\frac{1003}{p} = \sigma$ - the dimensionless pressure factor and substituting in equation/relation (7) we obtain that the association amongst the effective speed, s_{ef} and the pumping duration, t, becomes:

$$s_{ef} = \frac{V}{t} \cdot \sigma. \tag{8}$$

The ratio (V/s_{ef}) = τ, is commonly defined as a time invariant. Consequently, the pumping duration, t of a vacuum vessel from atmospheric load to a value of pressure p, will be:

$$t = \tau \cdot \sigma, \tag{9}$$

The dependency of the σ parameter on the wished-for pressure is presented in Figure 5. It must be mentioned that the pumping speed of ordinary pumps drops less than 10 mbar with gas ballast and less than 1 mbar without gas heft. This elementary attitude varies for pumps of different capacities, but it is recommended to not be overlooked in determining the pumping time relying on the pump size. It is emphasized that equations (6 to 9) and also Figure 5 apply only when the final pressure reached alongside the pump applied is several orders of amplitude lower than the wanted pressure.

Preprints (www.preprints.org) | NOT PEER-REVIEWED | Posted: 11 January 2024 doi:10.20944/preprints202401.0908.v1

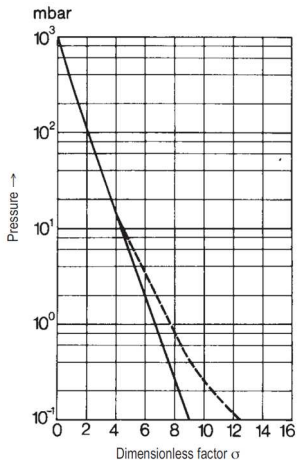

Figure 5. Dependence of the adimensional parameter, σ for the determination of the pumping duration, t according to equation (8) [15].

In the gross vacuum regime, the capacity of the chamber is determined for the duration engaged in the pumping routine. In the high and ultrahigh vacuum areas, the release of gases from the walls (of the corn seeds and the vessel) exhibits a significant function, in the medium vacuum region, the evacuating process is affected by both quantities. Additionally, in the medium vacuum zone, especially in the situation of rotary pumps, the maximum pressure that can be reached is no insignificant.

If the amount of gas accessing the chamber is established to be Q (in mbar·l/s) from the gas release from the seed enclosures, the chamber, and the leaks, the differential equation (5) for the pumping operation changes into [2]:

$$\frac{dp}{dt} = -\frac{s_{ef}(p-p_f)-Q}{V}, \tag{10}$$

and through the integration of this equation (11), we obtain:

$$t = \frac{V}{s_{ef}} ln \frac{(p_0-p_f)-Q/s_{ef}}{(p-p_f)-Q/s_{ef}} \tag{11}$$

Unlike equation/relation (7), equation/relation (11) does not allow for a definition of the solution for the effective pumping velocity, s_{ef}; therefore, the s_{ef} for a well-known gas release cannot be obtained derived from the pressure drop curve over time without additional knowledge, Figure 6.

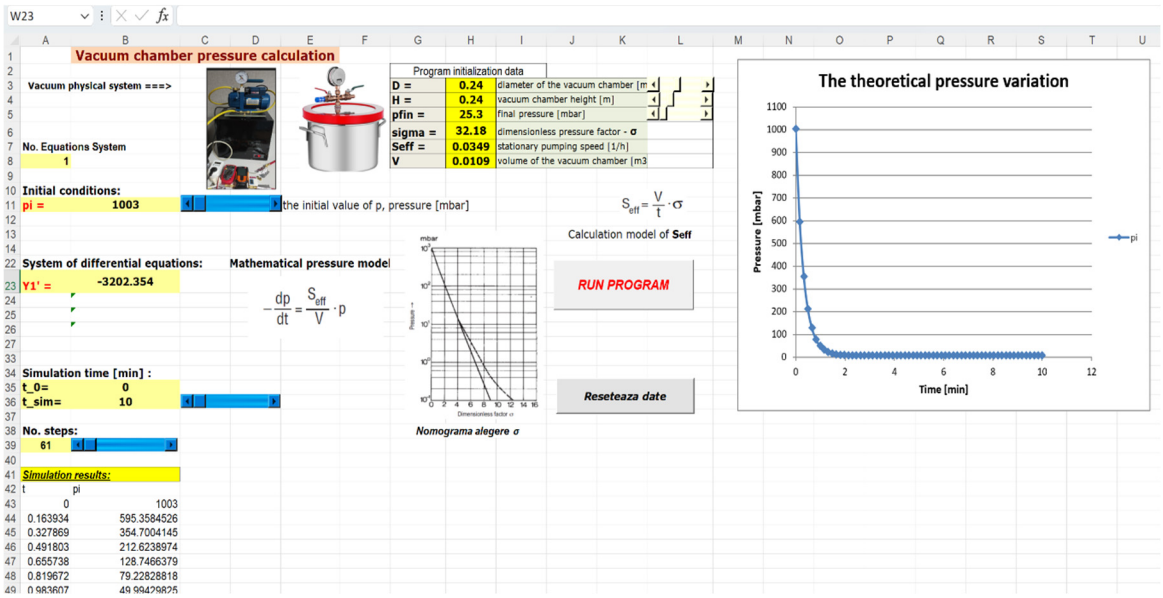

Figure 6. Graph of the gas load pressure versus time.

Preprints (www.preprints.org) | NOT PEER-REVIEWED | Posted: 11 January 2024 doi:10.20944/preprints202401.0908.v1

Therefore, in usage, the strategy will necessitate a pump with enough upward pumping speed, calculated from equation/relation (7) as an outcome of the volume of the gas-free chamber and the wanted pumping duration. Instead, the ratio Q/s_{ef} between the gas release velocity and this pumping speed is established. This ratio must be lesser than the needed pressure; for protection, it should be approximately ten times smaller. If the corresponding situation is not met, a pump with a comparable elevated pumping speed must be selected. In a situation where the pumping process is dominated by residual gas, pumping in a high vacuum region can be described by the relation [2]:

$$p = p_0 \cdot exp\left[-\frac{(s_{ef}/V_t)}{t}\right], \tag{12}$$

where: V_t - is the total volume of the system.

However, by far, the most significant uncertainty associated with pump performance, pressure, flow, and external leaks is due to gas release. Gas release rates can differ by several orders of amplitude, according to the component of a surface, its external intervention, humidity, temperature, and the exposure duration to vacuum. As it usually approaches asymptotically to the final pressure of a system, even small changes in gas loads result in significant differences in evacuation times (see Figure 6). Vacuum analysis, which aided in selecting a roughing pump, relied solely on the relationship between pressure and the time to reach this pressure, assuming the following relevant hypotheses for such an analysis: the system has no leaks, the pump is 100% productive, and nothing will vaporize in the vacuum vessels.

The calculation application was developed using Microsoft Excel, but any equivalent software to Microsoft Office that includes a spreadsheet with similar features to Excel can be used, making the adaptation of the application relatively easy. The choice of an Excel spreadsheet to simulate the variation of the vacuum system pressure over time is due to its capability to perform numerical description (in a table) applying symbolic statement as thoroughly as visual description using tables constructed for this purpose. The skill to activate and explore numerical, symbolic, and visual description dynamically makes the spreadsheet an essential instrument for promoting conceptualization and algebraic reflection [22]. Excel uses the VBA (Visual Basic for Applications) language, which is now widely used. It should be emphasized that VBA is a complex programming language. With its help, data can be manipulated, complex tasks automated, interactions with other Office applications can be performed, and much more [23], [24].

Using a spreadsheet, we can generate the graph of the precedent response (12) that reveals the relationship between the initial time, t, and the gas load pressure in the vacuum chamber, $p(t)$, Figure 7. At the aforementioned, it is also feasible to see the so-called state curves, which represent the parametric error of estimation based on experimental data at each moment of the system's operation.

Since the particular solution (12) is a function that depends on parameters, s_{ef} (pumping speed in steady-state), V (volume of the vacuum chamber), and implicitly by σ (the dimensionless pressure factor), as well as the initial pressure of the gas load, p_0, at the initial moment $t_0 = 0$, we will observe how graphic elements are constructed that can be interactively modified using sliders for the constructive parameters of the chamber, diameter (D), and height (H), Figure 7. The design of the spreadsheet itself is indispensable to the development of the calculation section.

It should be emphasized that VBA is a complex programming language. With its help, data can be manipulated, complex tasks automated, interactions with other Office applications performed, and much more [24], [25]. Consequently, the relevant VBA editor was used and adapted accordingly for processing and analyzing the results obtained from the simulation. The interface of the "Vacuum Chamber Pressure Variation Simulation.xls" program, on the "Pressure" page, is presented in Figure 8.

Preprints (www.preprints.org) | NOT PEER-REVIEWED | Posted: 11 January 2024 doi:10.20944/preprints202401.0908.v1

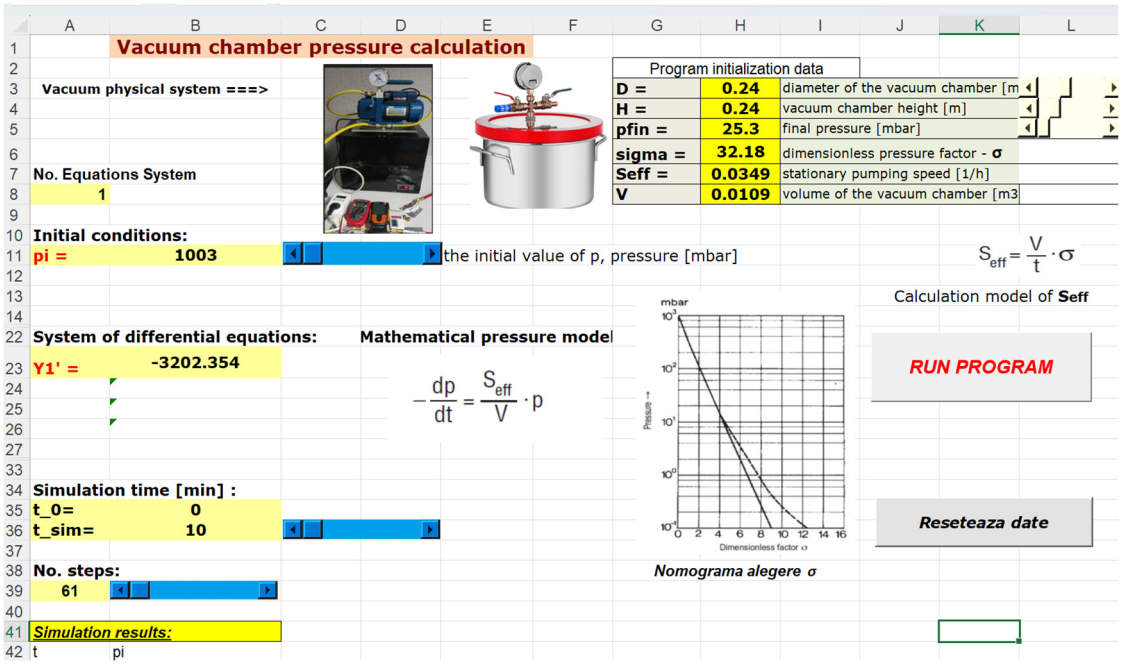

Figure 7. Display of the design and construction of the Excel spreadsheet.

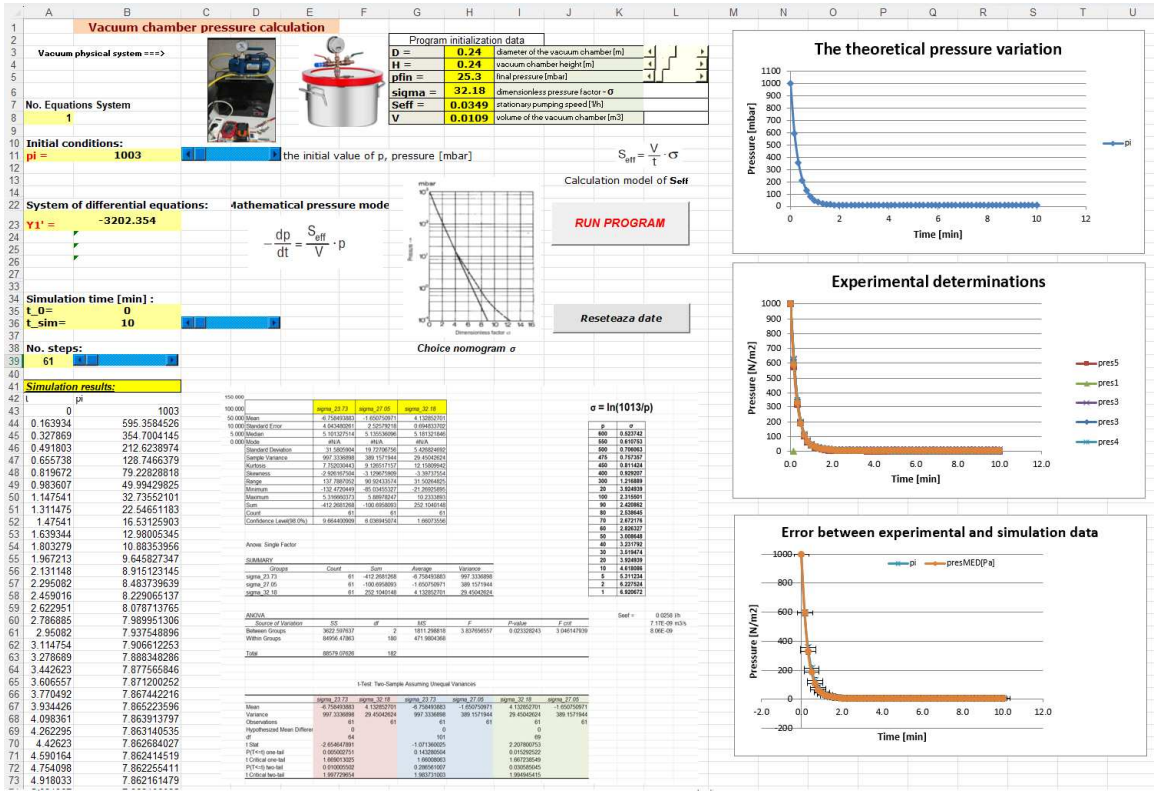

Figure 8. Interface of the "Vacuum Chamber Pressure Variation Simulation.xls" program; the "Pressure" page.

To identify the real or correct values, the absolute error (EA) was calculated. The real values were considered to be the mean values of the data resulting from multiple measurements in physical experiments with corn seeds. The measured average real value for the gas load pressure in the vacuum chamber was 44.273 mbar. The graph of the data obtained from measurements for the pressure variation over time is presented in Figure 9a. The estimated values of pressure over time for three different values of σ (dimensionless pressure factor), σ = 23.73; 27.05; 32.18, were calculated using the mathematical model adopted in the simulation program, and the data can be observed in

Preprints (www.preprints.org) | NOT PEER-REVIEWED | Posted: 11 January 2024 doi:10.20944/preprints202401.0908.v1

Figure 9b. The average values of the estimated pressures for each of the three data sets were 51.031, 45.920, and 40.140 mbar, respectively, with the estimated average value for all three data sets being 45.698 mbar. For each measurement, the following formula is applied to obtain EA:

$$EA = | \text{Estimated value} - \text{Real value} | \quad (13)$$

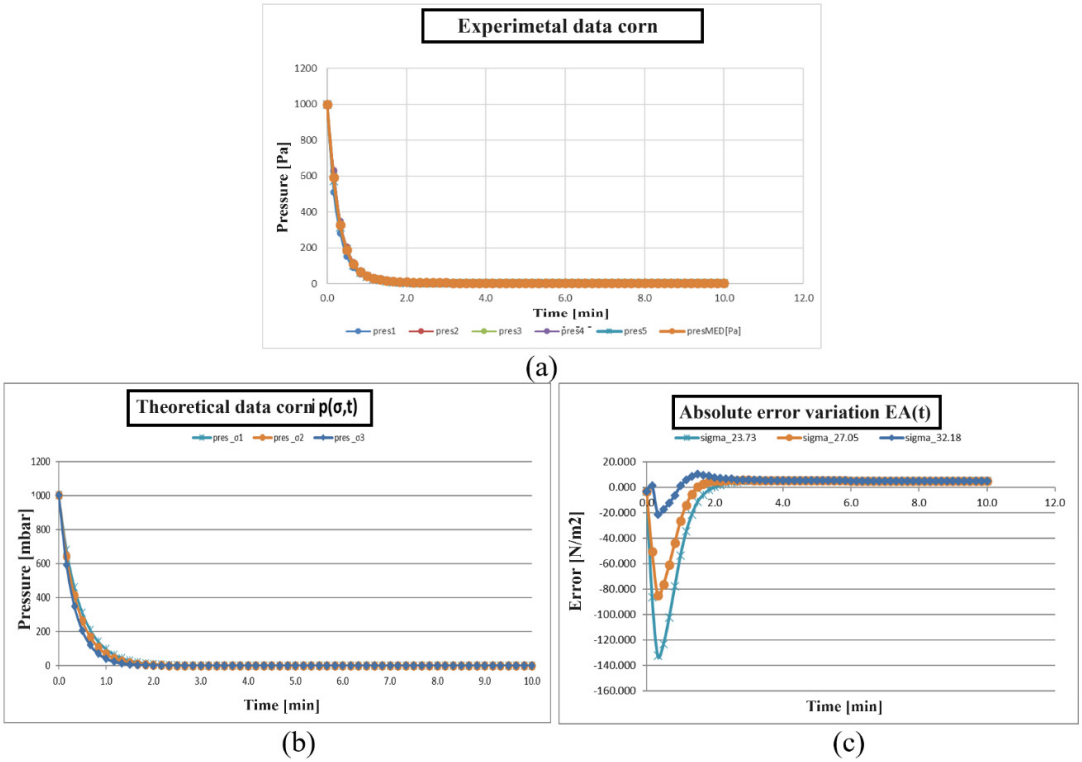

Figure 9. Execution launch of the simulation program and analysis of simulation accuracy.

The variation of EA for the three sets of estimated pressure data with the created simulation program is presented in Figure 9c. The trend of the error variation is similar for the three curves shown, with a peak at the moment $t = 0.33$ s. The highest peak value of 132.472 mbar was recorded in the dataset with $\sigma = 23.73$, while the lowest peak value of 21.269 mbar is encountered in the curve with $\sigma = 32.18$, and for $\sigma = 27.05$, the peak has a value of 85.035 mbar.

It is observed for all three curves that after approximately 2 minutes, the error value significantly decreases, reaching a steady-state value of about 5.161 mbar.

Then, if there are multiple measurements, errors can be summed to obtain the total EA or the average of absolute errors can be calculated by dividing the sum of absolute errors by the number of measurements. The calculation of the average EA for the estimated pressure with the simulation model was performed using the relation:

$$\text{Average:} \quad EA = (EA_1 + EA_2 + EA_3)/3 = (6.758+1.651+4.133)/3 = 1.425 \text{ mbar}, \quad (14)$$

Therefore, a very small value justifies the correlation between the results obtained through simulation and the real ones.

3.2. Experimental Procedure

For the structural dynamic analysis of the vacuum system under certain loads, the Finite Element Method (FEM) was used, considering the capabilities of the vessel made of stainless steel 316 and the lid made of acrylic plastic. The dynamic analysis process is carried out in the subsequent stage:

- The first stage is the selection of the material and some details. Several materials can be checked under vacuum pressure; however the most regular category spent are metals, plastics, and their

Preprints (www.preprints.org) | NOT PEER-REVIEWED | Posted: 11 January 2024 doi:10.20944/preprints202401.0908.v1

composites [18]. The ANSYS material library provided characteristic values for the materials of the chamber and the lid, as mentioned above, while the temperature and other experimental conditions are detailed below.

- The second step involves creating the 3D geometry of both the chamber vessel and the lid in the SolidWorks 2022 program (Figure 10) according to the dimensions (see Table 1) of the experimental physical model (see Figure 5).

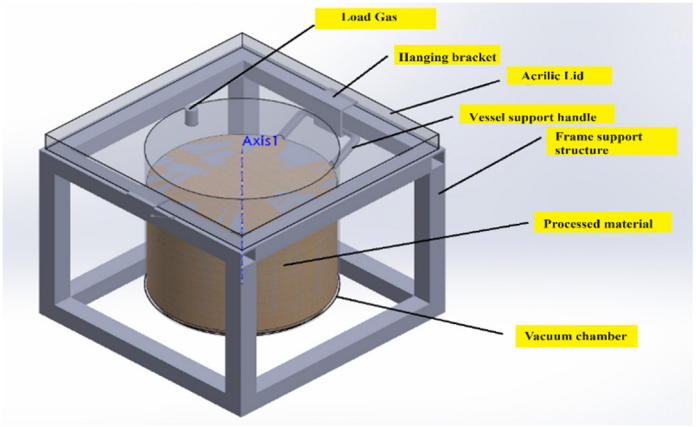

Figure 10. 3D geometric model of the vacuum system.

Modeling the contact-type connections between the vessel and the lid was automatically achieved through the Augmented Lagrange method for solving the nonlinear model of frictionless contacts (Figure 11a). The discretization was done automatically with default parameters for both the vacuum chamber and the chamber lid. Using the adaptive meshing method, a total of 10,546 nodes and 4,572 elements resulted (8,968 nodes and 4,363 elements for the vessel: 1,578 nodes and 209 elements for the lid). Modeling the constraints was done by fixing the lower edge of the cylindrical vessel. Modeling the loading with variable vacuum pressure over time, applied normally to the surface, according to the relationship, was also performed:

$$p = 10{,}1325 \cdot \exp(-0.023 \cdot t) + 40 \text{ [Pa]}, \quad (15)$$

This was achieved by selecting the interior surfaces of the vessel and the lid (see Figure 5b). The setting of the unit system was done by choosing the metric system (mm, kg, N, s, mV, mA, radians, rad/s, degrees Celsius).

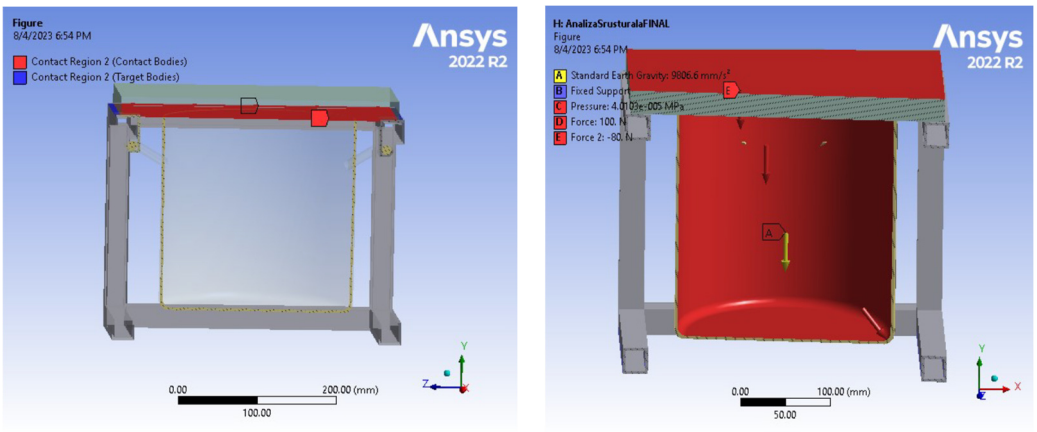

(**a**) (**b**)

Figure 11. Configuring the contact area between bodies: (a) the nonlinear model of frictionless connections; (b) the interior surfaces of the vessel and the lid.

The solution of the physical nonlinear model (without friction) in an average time of 2.45 minutes was performed on an Acer Swift 3 laptop with an Intel CORE I7 6500U processor at a

Preprints (www.preprints.org) | NOT PEER-REVIEWED | Posted: 11 January 2024 doi:10.20944/preprints202401.0908.v1

frequency of 2.5GHz, using 0.31GB of the available 8GB RAM. The information is available in the resolution statistical report, Figure 12. The convergence graphs of force displacement for the solution of the nonlinear problem are visualized in Figure 13.

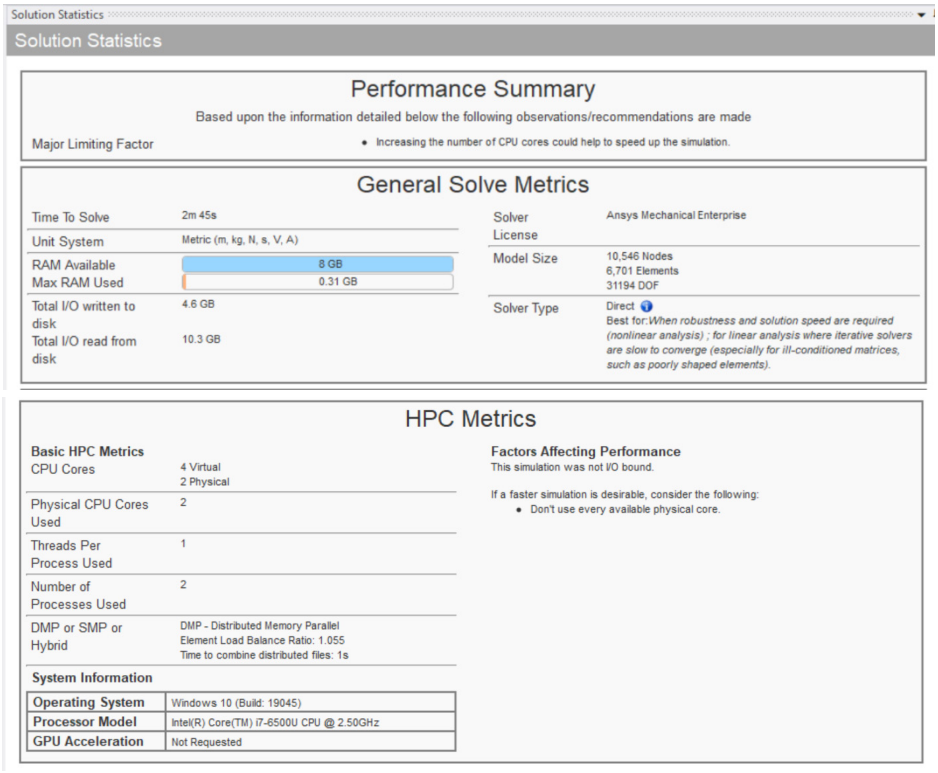

Figure 12. Statistical report of solving the nonlinear model.

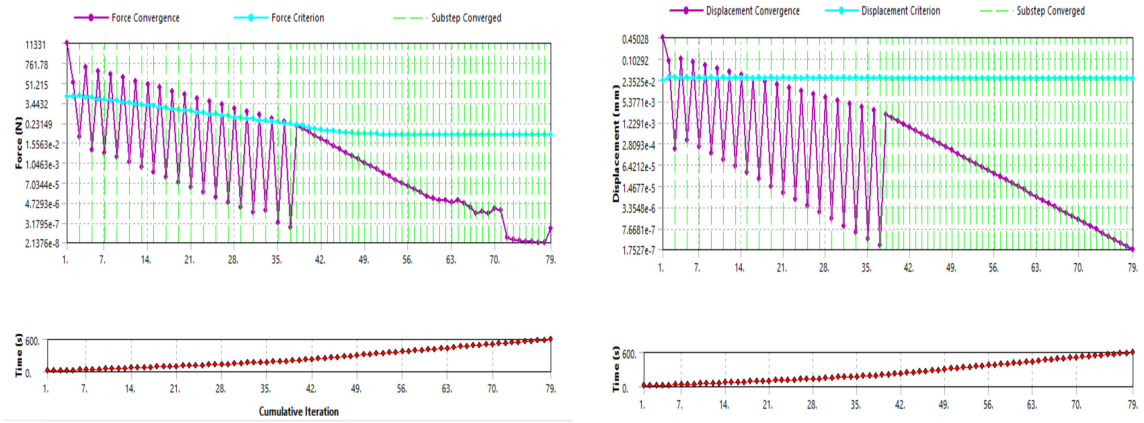

(**a**) (**b**)

Figure 13. Convergence of variables: (a) – force; (b) – displacement.

The image presented in Figure 14 illustrates the maximum deformation occurring at the bottom of the chamber as well as the deformation of the lid due to pressure. The maximum deformation of 0.009 mm was observed in the middle part of the lid and decreased radially towards the exterior. On the bottom of the vessel, we find deformations almost halved in order of magnitude, of about 0.004-0.005 mm, with the same decreasing radial distribution.

Preprints (www.preprints.org) | NOT PEER-REVIEWED | Posted: 11 January 2024 doi:10.20944/preprints202401.0908.v1

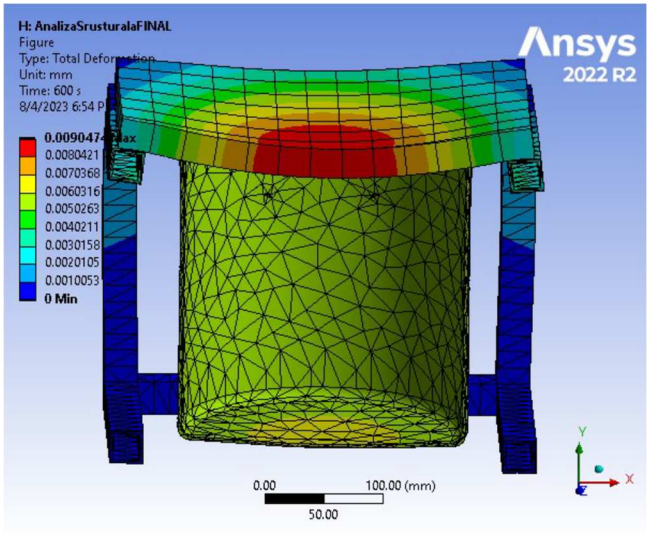

Figure 14. Deformations of the vacuum chamber wall and lid.

In addition, Table 2 summarizes the sample deformation values obtained by structural dynamic analysis depending on the pressure in the vacuum chamber of the test experiment.

Table 2. The total deformations produced by the vacuum pressure with the help of Ansys simulations.

Time [s]	Minimum [mm]	Maximum [mm]	Average [mm]
0	0	4.51E-01	2.82E-02
10		0.35917	2.24E-02
20		0.28578	1.78E-02
30		0.22737	1.42E-02
40		0.18093	1.13E-02
50		0.14403	8.97E-03
…		…	…
560		1.57E-03	1.03E-04
570		1.57E-03	1.03E-04
580		1.57E-03	1.03E-04
590		1.57E-03	1.03E-04
600		1.57E-03	1.03E-04

As the pressure stresses the walls of the vacuum chamber, Von Mises internal stresses occur in them due to the loading (compressive forces). According to Hooke's law, within the elastic limit, stress is directly proportional to deformation, and here the induced effort in the material of the walls and lid is the reaction to the applied compressive force [20]. The observed values of Von Mises stresses are presented both in tabular and graphical form. Figure 15a shows the stress distribution in the walls of the vacuum chamber and lid, with a maximum value in the central area of the vessel bottom due to stress concentration. Figure 15b depicts the variation of equivalent stresses over time, considering elastic loading, and the results are presented in Table 3, obtained using structural dynamic analysis.

Table 3. The equivalent of von Mises stresses as a function of time.

Time [s]	Minimum [MPa]	Maximum [MPa]	Average [MPa]
10	0.55818	63.982	9.9335
20	0.4394	50.826	7.8945
30	0.34646	40.381	6.2738
40	0.27352	32.094	4.9861
50	0.21614	25.52	3.9634
…	…	…	…
550	3.28E-04	0.23396	3.12E-02
560	3.25E-04	0.23391	3.12E-02
570	3.22E-04	0.23387	3.12E-02
580	3.20E-04	0.23384	3.12E-02
590	3.19E-04	0.23381	3.12E-02
600	3.17E-04	0.23379	3.12E-02

Preprints (www.preprints.org) | NOT PEER-REVIEWED | Posted: 11 January 2024 doi:10.20944/preprints202401.0908.v1

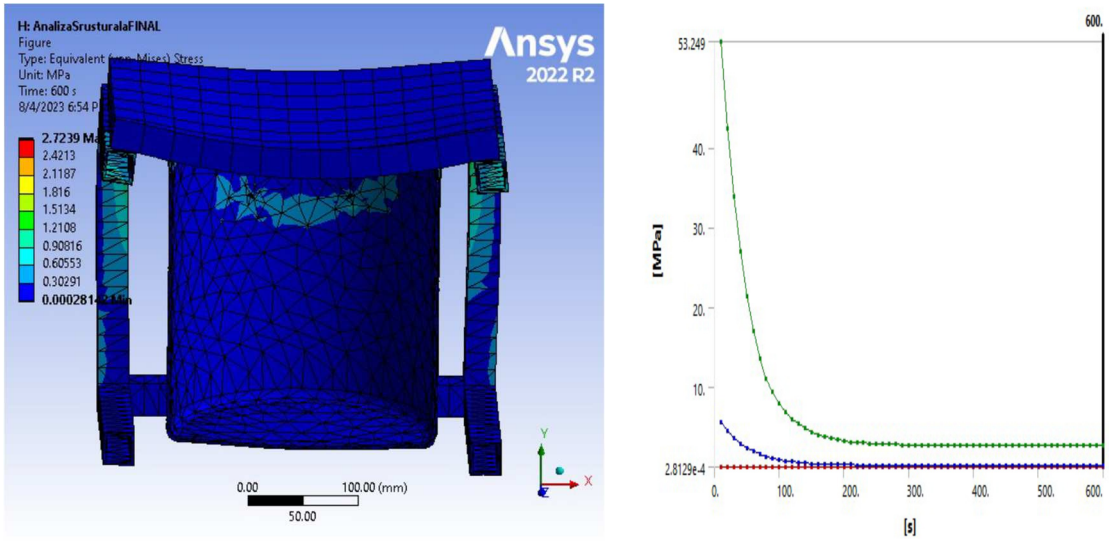

(**a**) (**b**)

Figure 15. 3D equivalent of von Mises stresses: (a) distribution on the chamber vessel and lid; (b) variation over time.

Following the analysis of the obtained results, as a result of their modeling and post-processing, the following highlights emerge:

- In the deformation process of the subassembly elements due to the action of vacuum pressure (Figure 5b), increased displacements are observed (max. 0.001569 mm) in the central area of the vessel bottom and (max. 0.000869 mm) in the central area of the lid.
- The equivalent Von Mises stress has increased values (max 63.92 MPa) in the body of the vessel in the middle area of the lower part, while on the lid, the values are insignificant.
- From the analysis of the maximum stress, the main compression load on the chamber body is highlighted, with a maximum value of 74.242 MPa in the connection area from the outside, and the tensile stress is reduced in the contact area with the body of the lid.
- The radial normal stresses, especially compression, have reduced values (52.643 MPa) in the joining area of the vertical wall of the vessel with the lower end portion;
- Increased values (21.434 MPa) of tangential (circumferential) stresses are highlighted in the body of the chamber in the area with the maximum diameter of its bottom, along with a significantly reduced tensile stress in the body of the lid;
- The total maximum value of the system energy over time was 617.65 mJ, with a predominance of 617 mJ in deformation energy and only 2.0225e-006 mJ in kinetic energy. A small deviation was acquired, demonstrating the validity of the conducted virtual experiment.

The significantly reduced values of the structural error field (max 2.4669 mJ) obtained for the chamber body indicate that the stress values are appropriate and close to the real ones. Additionally, Figure 15 highlights the rapid convergence (79 steps - see also Table 3) of the solution algorithm, and the computation time is reduced (an average of approximately 16.7 minutes cumulatively).

5. Conclusions

The numerical and experimental analyses conducted are considered vital for testing the material strength under various stresses. In this study, vacuum pressure testing was performed through dynamic Finite Element Method (FEM) analysis of the system designed for corn seed treatment. The equipment and specimens were designed according to ASTM D256 standards. All tests were conducted on materials: stainless steel 319 for the chamber vessel and acrylic plexiglass for the vacuum chamber lid.

The structural dynamic analysis accomplish using the FEM highlights that the chosen materials for manufacturing the vacuum chamber vessel and lid are durable and capable of withstanding the

desired pressure loads during seed treatment. The analysis results indicate the successful operation of the system. The effort illustration, table, and deformation graphs expose that the maximum deformation was found at the center of the lid and almost zero support handle due to the fixation on the frame.

For stress analysis, the outcomes express that the effort is maximum at the junction of the lower end of the vessel with the vertical wall. For deformation analysis, the results indicate that the deformation is the maximum at the center of the lower end of the vessel.

As a result of solving the nonlinear FEM model, adopting the convergence method for force and displacement, results with increased accuracy were obtained. The values of the obtained parameters (displacements, stresses, structural error) are useful for optimizing the shape and dimensions of the lid.

Reducing the mass of the vacuum chamber can be achieved under conditions of increasing maximum equivalent stress (but not exceeding the permissible value) and increasing the element's stiffness by solving the FEM model for optimization, adopting the gradient method for models with a single objective function and multiple constraints.

Statistical analysis of the correlation between experimental and estimated pressure values highlighted that both the proposed mathematical model and the solution method are well-chosen, with differences expressed through absolute error (EA) being very small.

Further research aims to analyze the experimental and numerical dynamics of the heating and cooling system in the degassing process of seeds in the vacuum chamber. Modal and harmonic analysis will be conducted to determine the natural frequency and mode shape of a structure, respectively, as well as the structure's response to variable harmonic loads over time.

Author Contributions: Conceptualization, G.I., F.I.; methodology G.I., F.I., V.F., G.V.; software, G.I., V.F.; validation, G.I., F.I., V.F., G.V.; formal analysis, V.F., G.V.; investigation, G.I., V.F., G.V.; resources, G.I., F.I.,V.F. G.V.; data curation, G.I., F.I.,V.F. G.V.; writing—original draft preparation, G.I.,F.I.; writing—review and editing, G.I., F.I.; visualization, G.I.,F.I., V.F., G.V.; supervision, G.I., F.I., V.F., G.V.; project administration, G.I., F.I.; funding acquisition, G.I., F.I.,V.F. G.V. All authors have read and agreed to the published version of the manuscript.

Funding: This research received no external funding.

Institutional Review Board Statement: Not applicable.

Informed Consent Statement: Not applicable.

Data Availability Statement: Data is contained within the article.

Conflicts of Interest: The authors declare no conflict of interest.

References

1. Jousten K., *Handbook of Vacuum Technology*, Second Edition, Wiley-VCH Verlag GmbH&Co.KGaA, **2016**, Weinheim, Germany.
2. Umrath W., Fundamentals of Vacuum Technology, Oerlikon Leybold Vacuum, **2007**, Cologne, Germany.
3. *** *The Vacuum Technology Book & Know how Book*, Volume II, Pfeiffer Vacuum GmbH, **2013**, www.pfeiffer-vacuum.com.
4. Silverio G-L., Chuck-Hernandez C., Serna-Saldivar S.O., Development and Structure of the Corn Kernel, *Corn (Third Edition)- Chemistry and Technology* **2019**, 147–163. DOI:10.1016/B978-0-12-811971-6.00006-1.
5. Govindaraj M, Masilamani P, Albert VA, Bhaskaran M. Effect of physcal seed treatment on yield and quality of crops: A review. *Agriculture Reviews* 2017, *38*(1), 1-14, DOI: 10.18805/ag.v0iOF.7304.
6. Farooq M.A, Ma W., Shen S., Gu A., Underlying Biochemical and Molecular Mechanisms for Seed Germination, *Int. J. Mol. Sci.* 2022, *23*, 8502, https://doi.org/10.3390/ijms23158502.
7. Ramdan E.P., Perkasa A.Y., Azmi T.K.K., Aisyah, Kurniasih R., Kanny P.I., Risnawati, Asnur P., Effects of physical and chemical treatments on seed germination and soybean seed-borne fungi, *IOP Conf. Series: Earth and Environmental Science* 2021, *883*,012022, DOI:10.1088/1755-1315/883/1/012022.

8. Sonhaji YS, Surahman M, Ilyas S, Giyanto, Seed treatment improved seed quality, seed production, and controlled downey mildew disease on sweet corn, *J. Agron. Indonesia* 2013, *41*(3), 242-248, http://repository.ipb.ac.id/handle/123456789/67027.
9. Deepa G.T., Chetti M., Khetagoudar M., Adavirao G., Influence of vacuum packaging on seed quality and mineralcontents in chilli (Capsicum annuum L.), *J Food Sci Technol.* **2013**, *50*(1),153–158, DOI 10.1007/s13197-011-0241-3.
10. Ramdan E.P., Arti I.M., Risnawati, Evaluation of viability and corn seed-borne pathogens in physical and chemical treatment, *J. Berkala Penelitian Agronomi* 2020, *8*(2),16-24.
11. Lawrence B., Bicksler A., Duncan K., Local treatments and vacuum sealing as novel control strategiesfor stored seed pests in the tropics, *Agron. Sustain. Dev.* **2017**, *37*, Article number 6, DOI 10.1007/s13593-017-0415-0.
12. Arbaugh B., Rezaei F., Mohiti-Asli M., Pena S., Scher H., Jeoh T., A Strategy for Stable, On-Seed Application of a Nitrogen-Fixing Microbial Inoculant by Microencapsulation in Spray-Dried Cross-linked Alginates, *ACS Agric. Sci. Technol.* **2022**, *2*, 5, 950–959, https://doi.org/10.1021/acsagscitech.2c00107.
13. Li L., Li J., Shao H., Dong Y., Effects of low-vacuum helium cold plasma treatment on seed germination, plant growth and yield of oilseed rape. *Plasma Sci. Technol.* **2018**, *20*, 095502, DOI 10.1088/2058-6272/aac3d0.
14. Kouki A., Theory of vacuum, **2022**, DOI: 10.13140/RG.2.2.33547.16160.
15. Marquardt N., Introduction to the principles of vacuum physics, *Inst for Accelerator Phys & Synchrotron Radiat, CAS - CERN Accelerator School: Vacuum Technology* **1999**, 1-24, e-proceedings: 10.5170/CERN-1999-005.
16. Lateş M-T., *Finite element method. Applications*, Transilvania University Publishing House Braşov - **2008** (in Romanian).
17. Butnariu S., Mogan Gh., *Finite element analysis in mechanical engineering. Practical applications in ANSYS*, Transilvania University Publishing House in Braşov - **2014** (in Romanian).
18. Jamil T., Azher K., Tahir M.A, Ali Z.,, Hameed W., Javed H.H., Experimental and numerical dynamic analysis of plexiglass acrylic for impact energy using indigenously developed testing equipment, *U.P.B. Sci. Bull., Series D* **2022**, *84*(3), 191-206.
19. Ipate G., Ilie F., Cristescu A.C., Finite element 3D numerical simulation study of car braking systems and brake disc/drum–pad/shoe friction couple materials, *TE-RE-RD, E3S Web of Conferences* **2020**, *180*, 03003, https://doi.org/10.1051/e3sconf/202018003003.
20. Tickoo S., Ansys Workbench 14.0: A Tutorial Approach, *Cadcim Technologies* **2014**.
21. Florin Gabriel Blaga F.G., *The dynamic action of the wind on multi-storey metal structures*. PhD Thesis, Technical University of Cluj Napoca – **2022** (in Romanian).
22. Oliveira M.C., Nápoles, S. Using a Spreadsheet to Study the Oscillatory Movement of a Mass-Spring System, *Spreadsheets in Education (eJSiE)* **2010**, *3*(3), Art.2, http://epublications.bond.edu.au/ejsie/vol3/iss3/2.
23. Ed Bott Ed., Woody Leonhard W., Special Edition Using Microsoft Office 2003, *Student-Teacher Edition* **2002,** Google Books.
24. Roman S., (2002). Writing Excel Macros with VBA, 2nd Edition. O'Reilly Media, Inc. **2002**.
25. Cooksey R., Descriptive Statistics for Summarising Data, *Illustrating Statistical Procedures: Finding Meaning in Quantitative Data* **2020** PMCID: PMC7221239, 61–139. DOI: 10.1007/978-981-15-2537-7-5.